Article

Simulation Study on Geometric Parameters Influencing the Flow Coefficient of Perforated Plate

Yaogen Peng [1], Huijun Mao [1,2,*], Zhichao Liu [1,2] and Cheng Wei [1,*]

1   School of Architecture, South China University of Technology, Guangzhou 510641, China
2   State Key Laboratory of Subtropical Building Science, South China University of Technology, Guangzhou 510641, China
*   Correspondence: armhj22@mail.scut.edu.cn (H.M.); weicheng@scut.edu.cn (C.W.)

Abstract: Natural ventilation is one of the vital means for passive energy-efficient design in green buildings. As a widely used building façade, the perforated plate is mostly utilized for appearance decoration, noise absorption, and sun shading, but its impact on the natural ventilation effect has rarely been paid attention to. In this study, the influence of the perforation rate, the perforation size, and the perforation shape on the flow coefficient of the perforated plate were simulated using the commercial CFD software Fluent, and the correlation between the flow coefficient and these geometric parameters was then regressed. The results show that the flow coefficient of perforated plate increases with the increase in perforation rate, which is slightly greater than that of ordinary building openings, and the corresponding flow coefficients of different holes rank as circle > square > triangle under the same conditions. The flow coefficient increases with the increase in the perforation size, and this effect is greater when the size is small. In addition, the flow coefficient is less affected by the size of round holes compared to triangular and square holes. The regression model indicates that both the perforation rate and the perforation size have a considerable positive influence on the flow coefficient, while the square and triangle holes have a negative influence on the flow coefficient compared with the circular hole. Moreover, the geometric parameters of perforated plates that have the greatest influence on flow coefficient are perforation rate, perforation shape, and size, in descending order.

Keywords: natural ventilation; perforated plate; flow coefficient; CFD simulation; multiple linear regression

1. Introduction

Natural ventilation, as an important economic technique, can improve indoor thermal comfort and reduce indoor pollutant concentration [1]. Compared with the artificial wind produced by fans and air conditioners, natural wind is easier to make people feel the fluctuation of wind speed due to its turbulence features of $1/f$ conforming to the physiological rhythm of the human body, leading to increased thermal comfort [2,3]. Additionally, in the context of building energy consumption continues to rise (the building sector consumes 40% of the global primary energy) [4,5], the proper utilization of natural ventilation in buildings can significantly reduce the energy consumption of air conditioning and mechanical ventilation, and has great energy saving potential [6,7], thus reducing building heat dissipation and mitigating urban heat island [8,9]. Experimental tests carried out on two school buildings in southern Spain demonstrated that using a natural ventilation system resulted in a significant reduction in energy consumption over the academic year compared to using a mechanical ventilation system. With the natural ventilation system, the main energy savings ranged from 18% to 33% while keeping comfort levels in the classroom [10].

Numerous studies have shown that the effect of natural ventilation largely depends on design elements such as building layout and orientation [11,12], while the shape of the

building opening and installation position are also key factors affecting the efficiency of natural ventilation [1]. The flow coefficient of the building opening is a significant factor that affects the effect of natural ventilation and is crucial in determining the ventilation rate and the distribution of the indoor thermal environment [13]. A few of the earlier studies hold that the flow coefficient of natural ventilation is constant. For example, ASHRAE Handbook [14] regards the flow coefficient as a constant, which ranges from 0.60 to 0.65, which is likewise thought to be a constant by Hunt et al. [15], and Li, Y. G. et al. [16]. However, the majority of studies note that the flow coefficient is not a constant, but varies with the location of the building opening, the opening area, the wind direction, and other factors. Hildebrando et al. [1] carried out a site measurement to evaluate the flow coefficient of open windows, and the results showed that a side-hung casement window with a roller shutter may have a discharge value that ranges from 0.41 to 0.81. Using a modeled, naturally ventilated dairy building by computational fluid dynamics (CFD) simulation, Yi et al. [17] examined the effects of wind speed and wind direction on the flow coefficient of the windward sidewall opening with different opening sizes. According to the findings, outdoor wind speed had almost no effect on the flow coefficient, but wind direction exhibited a significant impact. In addition, Ahsan et al. [13], Liao et al. [18], and Wang et al. [19] have also come to similar conclusions.

Perforated plate is a prevailing architectural skin design, providing an aesthetic view, noise absorption, and sun shading, which is favored by many architectural designers [20]. Chi, D. A. et al. [21] presented a methodology to predict a set of optimum perforated plate design variables to increase daylighting performance in office buildings located in Seville, Spain. In comparison to reference models without perforated plates, the actual daylit area was raised by 29–57%, and the overlit area was decreased by 36–57%. Jesus M. et al. [22] studied the thermal performance of the perforated plate taking into account several physical parameters, including perforation rate, color and material, and the impact of wind penetration. The improvement in energy savings that various combinations of these parameters could have on the building as a whole was also quantified by this research. The mechanical characterization of perforated façades has also been analyzed [23].

However, less attention has been paid to the ventilation performance of perforated plates. Due to the low perforation rate, its obstructing effect on airflow cannot be ignored. Few systematic studies have been conducted on the ventilation performance of perforated plates, which results in a dearth of pertinent information for appropriate selection. Miguel [24] investigated how the geometry of the holes and the void percentage of plates affect fluid flow in perforated plates, and the results suggested that circular-holed perforated plates were probably less effective at transporting liquids than noncircular-holed plates, which provided vital information for the efficient design of perforated plates. Tahsin et al. [25] and Phillip et al. [26] also quantified the correlation between fluid flow and pressure loss for perforated plates. Li [27] studied the additional resistance characteristics of the ventilation system caused by perforated plates and analyzed the relationship between additional resistance and distance within the range of perforation rate of 20–50% and distance of 100–1000 mm. Nevertheless, with the evolution of the perforated plate, its perforation rate, hole type, and aperture have changed as well, making it difficult to rapidly and precisely determine the flow coefficient of perforated plate.

In addition, the complex structure of building openings will significantly increase the number of grids and costs in the building ventilation simulation [28,29], such as sliding windows, shutters, hung windows, etc. Similarly, the perforated plate will also greatly increase the complexity of the geometric model. In order to consider its obstruction effect on air flow, it is necessary to carry out mesh refinement for a large number of holes, which makes the computation cost to be exceedingly expensive. However, if the flow coefficient of a certain perforated plate can be determined, the perforated plate can be simplified to an ordinary building opening, and its flow coefficient can be utilized as a boundary condition, thereby saving pre-processing time and computing resources. Therefore, a

detailed understanding in this respect is needed in-depth, which is crucial in the reasonable selection of perforated plates and simplification of natural ventilation simulation.

Because outdoor weather conditions are unpredictable and it is challenging to acquire the desired wind speed and wind direction, field measurements are not practical to study the flow coefficient [30]. Although wind tunnel experiments can create controllable wind conditions [31], they can be labor- and time-intensive if there are many different experimental scenarios. By contrast, in the study of ventilation, CFD modeling is a quick and parameter-controllable method. Information on the entire airflow and pressure fields can be acquired using the validated CFD simulation [32]. As a result, this study used the CFD methodology.

Therefore, this study aims to explicit the impact of the perforation rate, the perforation size, and the perforation shape on the flow coefficient, investigate the quantitative correlation between the flow coefficient and the geometric parameters of the perforated plate, and explore the application value of the regression model in practical engineering.

2. Methods

2.1. CFD Validation

The experimental data by Huang et al. [33] for a perforated orifice was used to validate the numerical model. In the experiment of Huang et al. [33], the flow coefficients for different structures (orifice thickness, porosity, hole distribution, and upstream disturbance) were evaluated. In detail, perforated plate No.12 was selected, as illustrated in Figure 1. Upstream, downstream, and central (perforated plate) regions make up the geometry. With smooth flow states, the upstream and downstream regions have mesh with coarser grids. Finer meshes are used to capture high velocity and pressure distributions in the center of the perforated plate, and meshes close to the wall are also refined to satisfy requirements for standard wall functions.
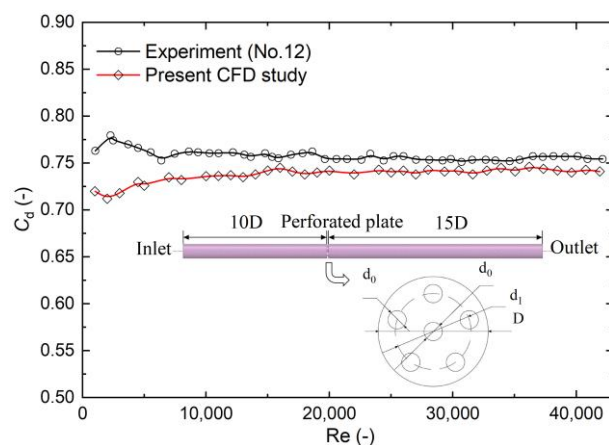

Figure 1. Comparison between experimental and numerical results of the discharge coefficient.

The continuity, momentum, and energy equations with the realizable k-ε model closure are deployed to resolve the turbulent flow near the perforated plate. The k-ε two-equation turbulence model has been widely used in simulating the turbulent flow, and the realizable k-ε model has significantly outperformed the standard k-ε model in characterizing flows with strong streamline curvature, vortice, and rotation [32,34]. Figure 1 compares the simulated flow coefficient C_d with the experimental values, with water as the working fluid. It can be found that the numerical results give lower values than the experimental magnitudes, especially in the low Reynolds number region. However, the overall average deviation (2.1%) is less than 5% for all simulated cases, suggesting that the simulation method can accurately predict the flow coefficient of the perforating plate.

2.2. Physical Models

2.2.1. Geometric Model and Boundary Conditions

　　Figure 2 shows the geometry and meshing of the computational model, which has a domain (Figure 2a) composed of three parts: the upstream section, the perforated plate section, and the downstream section. The length of the upstream section and the downstream section is 0.7 m, with a width of 0.2 m and a height of 0.4 m. Studies have shown that the air velocity and pressure measurement positions have a significant impact on the simulation results, and they should be located in the fully developed flow, which is a prerequisite for calculating the flow coefficient [35]. The reason is that after passing through the perforated plate, the flow pattern will change dramatically, and its interference distance is not just restricted to the perforated plate part but also extends further downstream. The air velocity and pressure measurement positions were determined through preliminary simulation, and the distributions of velocity and pressure near the measurement positions were steady and uniform (Figure 3), satisfying the requirement for flow coefficient calculation.
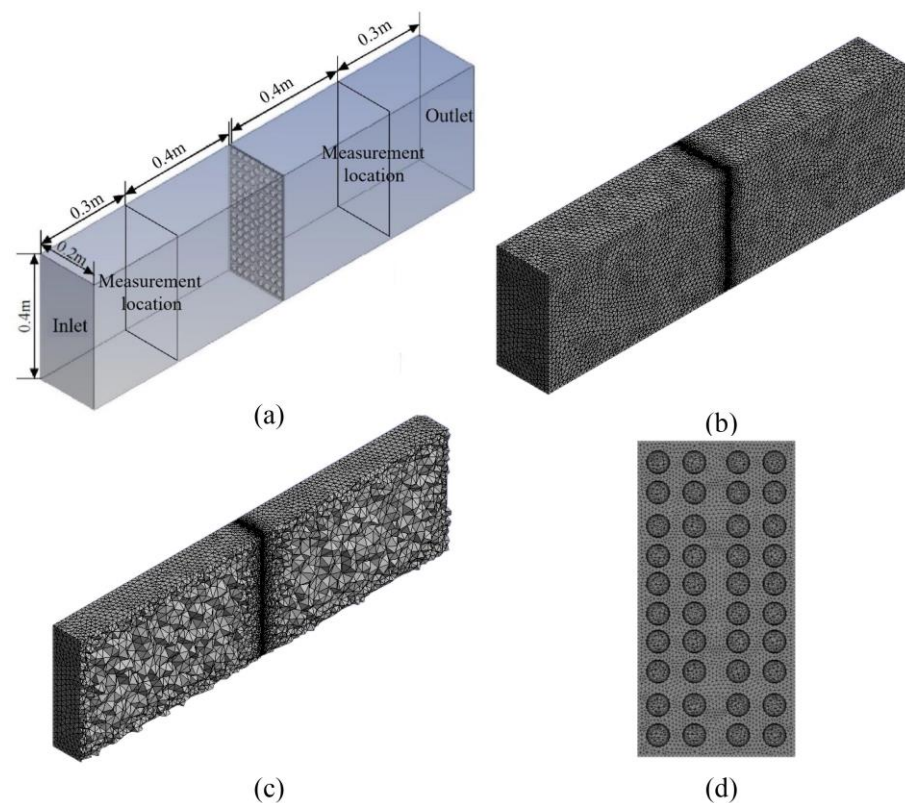

Figure 2. Illustration of (**a**) the geometric model, (**b**) mesh generation, (**c**) vertical section plane of mesh, and (**d**) mesh near the perforated plate.
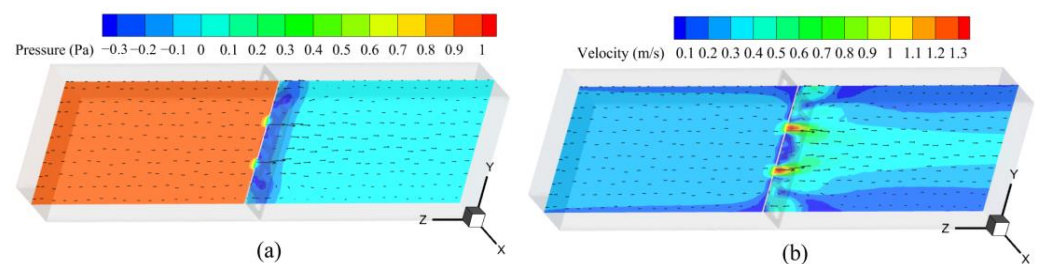

Figure 3. The distributions of (**a**) pressure contour and (**b**) velocity vector.

As for the setting of boundary conditions, both the inlet and outlet were specified as pressure control surfaces by referring to previous studies [35,36], with the inlet and outlet conditions of pressure-in and pressure-out, respectively, and the pressure difference between the inlet and outlet was 1 Pa. Solid wall boundary condition was utilized for the four surfaces except for the inlet and outlet, and non-slip velocity boundary conditions were applied at the solid surfaces. The fluid medium was set as air with a viscosity of 1.7894×10^{-5} kg/(m·s) and a density of 1.225 kg/m^3, respectively.

2.2.2. Numerical Scenarios

Perforation rate, perforation shape, and perforation size are the basic geometric characteristics of the perforated plate. The perforation rate refers to the proportion of the total area of the perforated holes in the overall area of the perforated plate; as shown in Figure 4a, a perforation rate of 25% is obtained by dividing the total area of all circular holes by the area of the plate. Too low of a perforation rate will negatively affect the aesthetic appearance and ventilation performance, whereas one that is too high will cause a sharp increase in stress and deflection and a reduction in safety. Account to relevant research, the reasonable range is generally 20–45% [26].
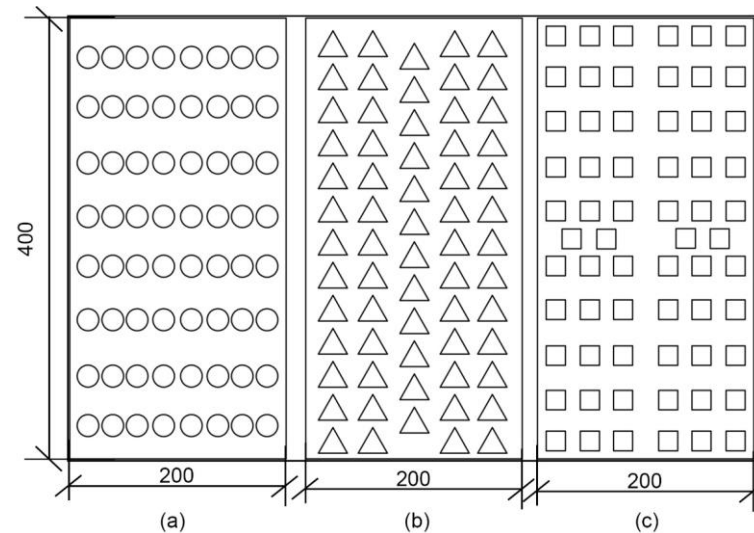

Figure 4. Plane and dimension comparison of (**a**) circular, (**b**) triangle, and (**c**) rectangle perforated plates, with the perforation rate of 25% (in mm).

Moreover, Li [37] found the perforated size used in engineering projects was concentrated in the range of 10–30 mm, with circular, triangular, and square holes making up the majority of the perforation shapes, as shown in Figure 4. In this study, we only considered the linear layout of the holes, while the staggered layout was not yet taken into account. It should be noted that part of the holes was not strictly in a line pattern in order to maintain the same perforation rate for different shapes of perforated plates, such as in Figure 4c. Regarding perforation size, for a circular hole, the perforation size refers to its diameter, while the perforation size is related to the side length for square and triangular holes.

Therefore, the simulation in this study totally considered 42 scenarios, including 18 scenarios for perforation size, 15 scenarios for perforation rate, and 9 scenarios for perforation shape (Table 1). In detail, for group A, six perforation rate scenarios—assuming a circle-shaped hole—were utilized for each perforation size (10, 20, 30 mm), so there are 18 scenarios in group A. As for group B, five perforation rate scenarios were considered for a circular perforated plate with a perforated size of 20 mm (triangle perforated plate with a perforated size of 27 mm and square perforated plate with a perforated size of 18 mm); hence, there are 15 scenarios in total. Likewise, for group C, three perforation sizes were defined for circular, triangle, and rectangle holes, assuming a 20% perforation rate.

Table 1. Simulated scenarios setting.

Group	Perforation Size (mm)	Perforation Rate (%)	Perforation Shape
A	10, 20, 30	20, 25, 30, 35, 40, 45	Circle
B	20 27 18	20, 25, 30, 35, 40	Circle Triangle Square
C	10, 20, 30	20	Circle Triangle Square

2.2.3. Mesh Independence

Meshing is a crucial stage that affects the accuracy of CFD simulation; the accuracy of the simulation-based results was significantly influenced by the mesh quality. Considering there are strong velocity and pressure gradients near the wall, Y plus grid-adaptation method was first used to refine or coarsen grids in the boundary area. In addition, velocity gradient grid adaptation was utilized to refine grids near the perforated plate, because there are often considerable changes in flow velocity and pressure there.

The three mesh sizes that were successively refined by about 1.2 at each dimension are used to investigate the grid sensitivity, and the number of tested cells was 85,883 (G1), 148,406 (G2), and 256,445 (G3), respectively. The performance time on 8 compute nodes for mesh G1–G3 are: 5.2, 14.5, and 25.8 min, respectively. Figure 5 shows the pressure and velocity distribution on the mid-line of the domain; although there is no difference in pressure (Figure 5a), there is a difference in velocity. As illustrated in Figure 5b, the results of the medium grids are similar to those of the fine grids, while the velocity curves of the coarse and fine grids are distinct. Considering both accuracy and computational efficiency, G2 exhibits good performance in these two aspects. Therefore, the mesh size G2 was adopted for the rest of the numerical scenarios.
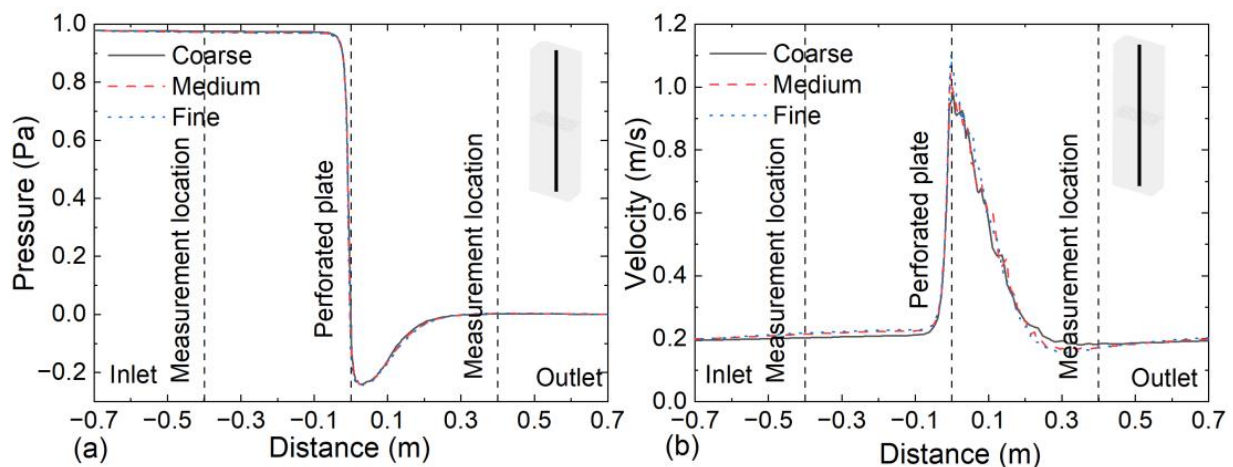

Figure 5. Comparison of pressure and velocity distribution for three mesh sizes, (**a**) pressure magnitude and (**b**) velocity magnitude over the middle line (line location as shown in the figure).

2.3. CFD Governing Equations

The commercial CFD program ANSYS Fluent 2020R1, a finite-volume-based fluid dynamics solver, was used to perform numerical simulations. Transport equations for incompressible flow have the following general form:

Continuity equation,

$$\frac{\partial p}{\partial t} + \nabla \cdot \left(\rho \vec{V} \right) = 0 \tag{1}$$

Momentum conservation equation,

$$\frac{\partial \vec{V}}{\partial t} + \left(\vec{V} \cdot \nabla\right)\vec{V} = \Gamma \nabla^2 \vec{V} - \frac{1}{\rho}\nabla p \tag{2}$$

where fluid velocity $\vec{V}$ at any point in the flow field is described by the local velocity components u, v, and w. Γ is a general diffusion coefficient, and t represents time.

The COUPLED algorithm was adopted to couple the pressure and velocity fields in the Reynolds-averaged Navier–Stokes (RANS) equations. The realizable k–ε model with enhanced wall treatment was used to model turbulence and simulate the near-wall flow. Convection and diffusion terms for flow variables were solved using a second-order discretization scheme. The convergence was to be obtained when residuals reached 1×10^{-4} for continuity, velocity, turbulent kinetic energy (k), and turbulent dissipation rate (ε) [32].

2.4. Determination of the Flow Coefficient

Under natural ventilation, the airflow through a building compartment can be regarded as an incompressible flow. Equation (3), derived from the Bernoulli equation, relates the pressure difference across the perforated plate (ΔP), with the pressure loss coefficient (ξ), the flow density (ρ), and the average flow velocity through the perforated plate (v). This equation is often presented in the form of Equation (4), in which C_d is the flow coefficient of the perforated plate.

$$\Delta P = \xi \frac{\rho v^2}{2} \tag{3}$$

$$Q = C_d A \sqrt{\frac{2\Delta P}{\rho}} \tag{4}$$

$$C_d = \sqrt{\frac{1}{\xi}} \tag{5}$$

Combining Equations (3)–(5), the flow coefficient can be expressed as follows.

$$C_d = \sqrt{\frac{\frac{1}{2}\rho v^2}{\Delta P}} \tag{6}$$

where $\frac{1}{2}\rho v^2$ represents the dynamic pressure through the perforated plate. Therefore, the pressure difference across the perforated plate and the dynamic pressure of the perforated plate in a fully developed flow can be extracted in the software so as to calculate its flow coefficient.

3. Results

3.1. Impact of Perforation Rate on Flow Coefficient

Figure 6 depicts the effects of perforation rate on the airflow distributions at the vertical middle plane across the domain for a circular-hole perforated plate with a perforation size of 20 mm. As the perforation rate increases, the interference distance of the perforated plate decreases gradually. Therefore, the determination of the measurement positions is reasonable due to the fact that the measurement positions were established by the preliminary simulation whit a 20% perforation rate. When it comes to the velocity distribution, an increase in perforation rate results in a more uniform velocity distribution in the downstream region, as shown in Figure 6a–c; this means that, when used in practice, a perforated plate with a higher perforation rate can result in a more uniform indoor velocity distribution, which is helpful for enhancing indoor comfort. Moreover, the wind speed through the perforated plate will increase as the perforation rate increases (see Figure 6d–f),

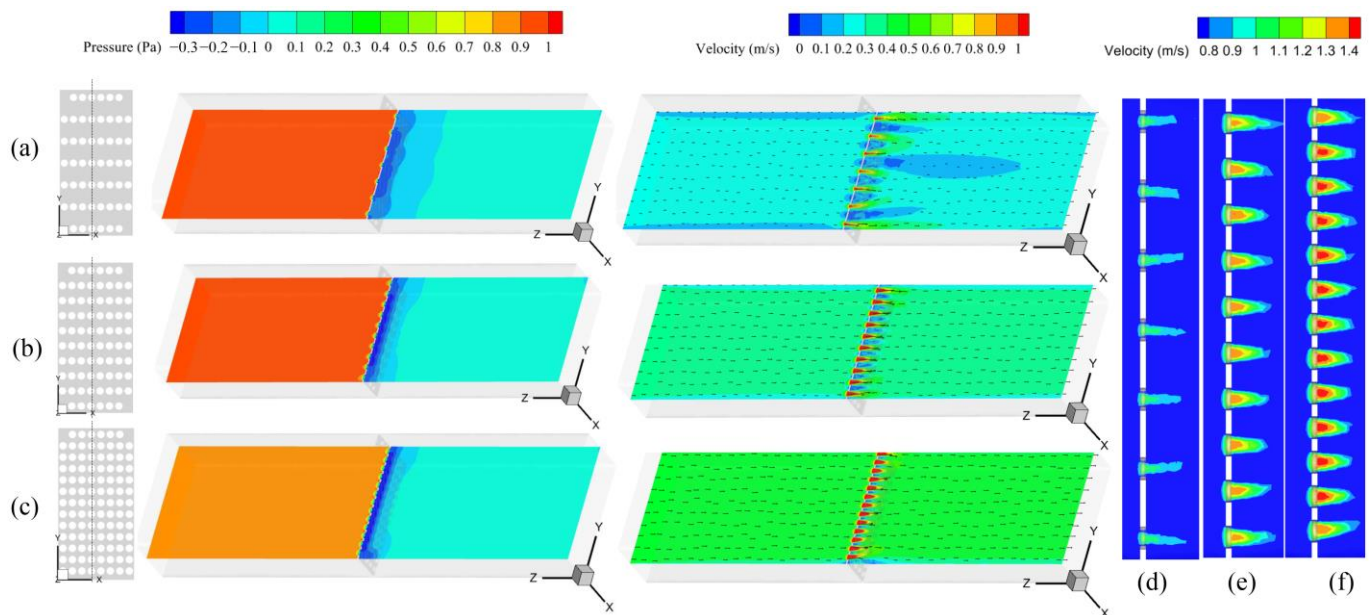resulting in an increase in dynamic pressure; thereby, the flow coefficient goes up according to Equation (6).

Figure 6. Comparison of contours of pressure and velocity distribution corresponding to different perforation rate of circular perforated plate, (**a**) α = 20%, (**b**) α = 30%, and (**c**) α = 40%, and comparison of velocity distribution near the perforated plate, (**d**) α = 20%, (**e**) α = 30%, and (**f**) α = 40%.

The flow coefficient of the perforated plate can be determined from the known velocity and pressure difference based on Equation (6). Figure 7 shows the variation of the flow coefficient corresponding to the circular perforated plate with a 20–45% perforation rate. It can be seen that with the increasing perforation rate, the flow coefficient also increases, which reveals that the flow coefficient is not a constant. The variation range for a perforated plate with 20 mm aperture, for instance, is 0.84–1.05, with a maximum variation rate of about 25.0%. According to a theoretical analysis by Gong et al. [38], the flow coefficient of large opening buildings under wind pressure is approximately 0.82–1.41, and the flow coefficient of perforated plates is within this range. This suggests that the simulation results in this paper are accurate.
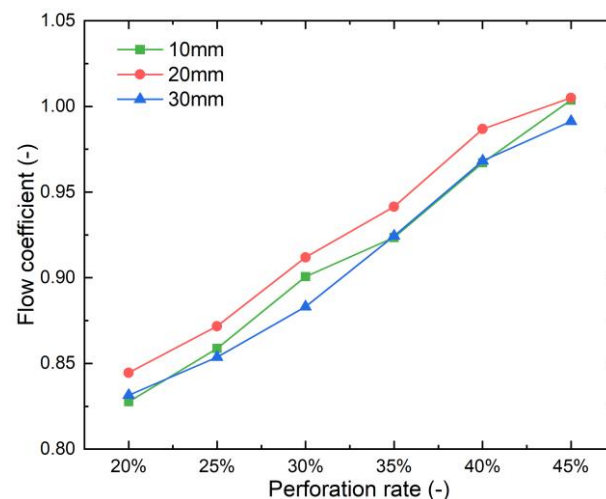

Figure 7. The flow coefficient corresponding to different perforation rates of circular perforated plates.

However, compared with the flow coefficient ranges of the side-hung window and bottom-hung window (0.65–0.77 and 0.78–1.00, respectively) [39], the flow coefficient of the perforated plate is slightly greater than that of ordinary building openings. The reason could be that there is less vortex between the perforated plate and the solid wall, which results in less flow resistance, and that the holes in the perforated plate are close together, causing air flow through them to interfere with one another and producing an "ejection siphon" effect. As a result, the overall flow coefficient of multiple holes will be greater than the ordinary openings with the same total area. This phenomenon has been confirmed in other studies as well. Ahsan et al. [13] found that the flow coefficient value was close to unity for smaller sash opening angles and declined as the sash opening angle increased.

3.2. Impact of Perforation Shape on Flow Coefficient

Figure 8 shows the pressure and velocity distribution of perforated plates with three shapes under the premise that the perforation rate is 35% and the single-hole area is the same. It can be observed that the perforated plates with different hole shapes and the same perforation rate have little impact on the uniformity of the downstream velocity field, but the interference distances of the pressure field are different. Moreover, the velocity near the hole of the circular perforated plate is higher than rectangle and triangle plates, as displayed in Figure 8d–f.
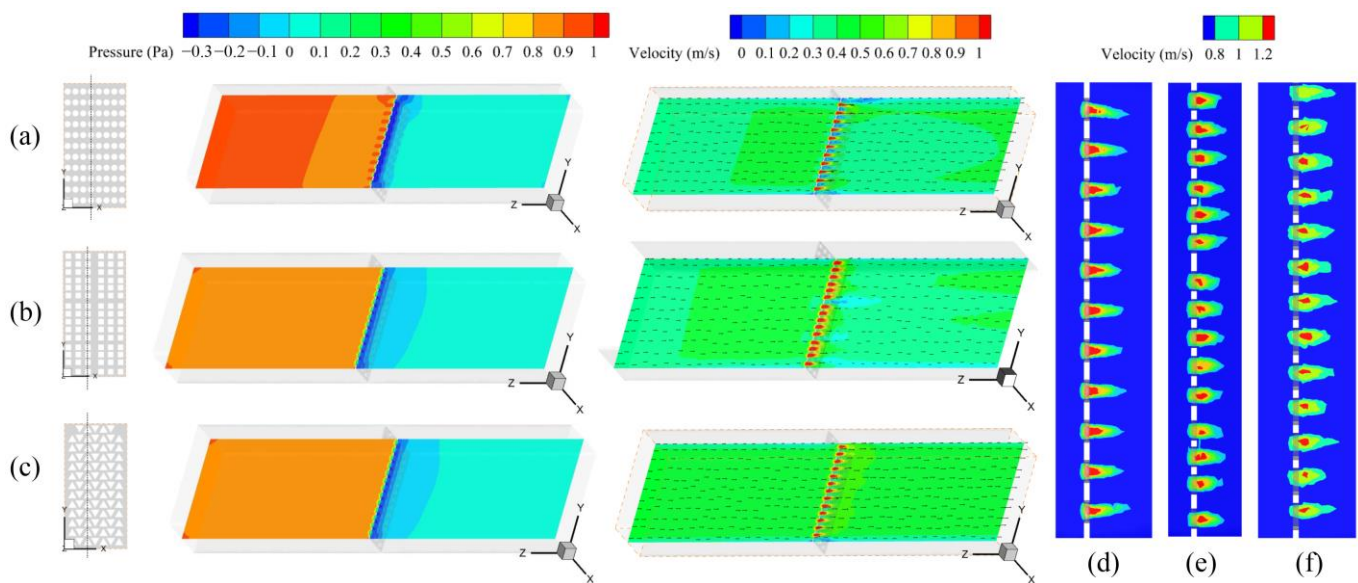

Figure 8. Comparison of contours of pressure and velocity distribution corresponding to different perforation shapes, (**a**) circle, (**b**) square, and (**c**) triangle, and comparison of velocity distribution near the perforated plate, (**d**) circle, (**e**) square, and (**f**) triangle.

As depicted in Figure 9, the flow coefficient of perforated plates increases together with the perforation rate. The variation law of the flow coefficient corresponding to the triangular and square holes is similar, but it differs significantly from that of the perforated plate with circular holes. In detail, the flow coefficients of perforated plates with triangular, square, and circular holes vary from 0.76 to 0.88, 0.78 to 0.89, and 0.84 to 0.99, respectively, with a perforation rate of 20% to 40%. Obviously, under the same conditions, the corresponding flow coefficients of different holes rank as circle > square > triangle, indicating that the circular hole can achieve higher flow coefficients and improve the effectiveness of natural ventilation. The reason is that when the cross-sectional area of a single hole is equal, the equivalent diameter of a circular hole is larger, which will reduce the flow resistance, thereby increasing the flow coefficient. This result is consistent with the findings of other researchers. In his detailed theoretical analysis of the flow coefficient of inlet and outlet

openings, Andersen [40] hypothesized that the value of C_d for sharp-edged openings was in the range of 0.55–0.65, while the value for round openings was 0.9–0.95.
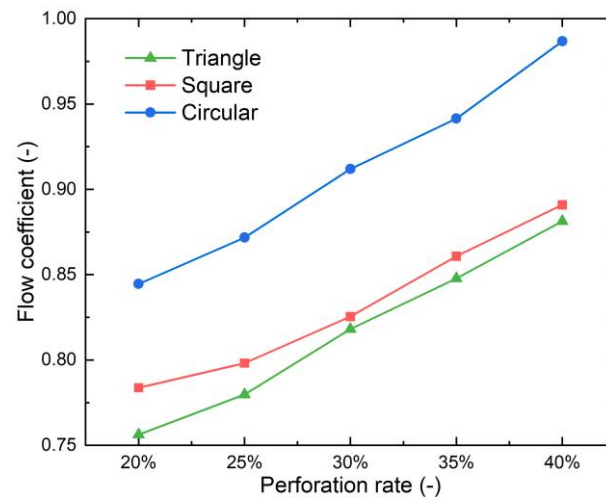

Figure 9. The flow coefficient corresponding to different perforation rates of triangular, square, and circular perforated plates.

3.3. Impact of Perforation Size on Flow Coefficient

Figure 10 displays the flow coefficients corresponding to different perforation sizes of perforated plates with three shapes. On the premise of the same perforation rate and hole shape, it can be seen that the flow coefficient increases with increasing perforation size, which means the obstruction effect on the airflow weakens. Additionally, the impact of the perforation size on the flow coefficient is greater when the perforation size is small. For triangular perforated plates, the flow coefficient varies by 0.13 when the perforation size goes from 10 to 20 mm, but only by 0.08 when it increases from 20 to 30 mm.
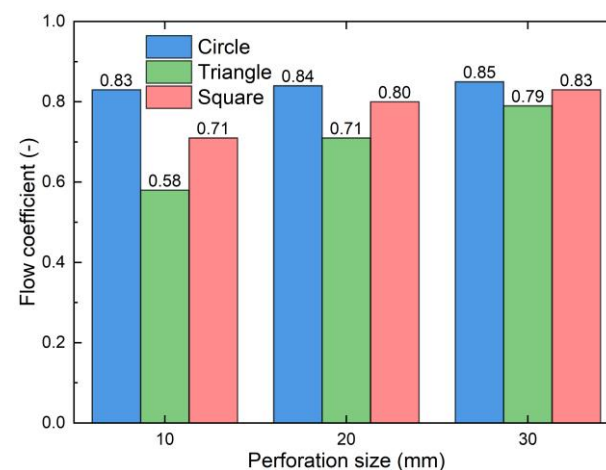

Figure 10. The flow coefficient corresponding to different perforation sizes of triangular, square, and circular perforated plates.

However, the perforation size has little effect on the flow coefficient of the perforated plate when the perforation shape is circular. Regardless of whether a perforation is a triangle- or square-shaped, the perforation size greatly affects the flow coefficient of the perforated plate, indicating that a larger flow coefficient can be obtained by using a larger hole. The shading, lighting, and ventilation effects should be comprehensively considered when selecting perforated plates, but their interactions have not been fully understood [41]. Despite this, it is evident from the aforementioned conclusions that for the perforated plate

with circular holes, the perforation size has no bearing on its ventilation effect and that the only relevant factor is the conflict between shade and sunlight.

3.4. Correlation between Flow Coefficient and Geometric Parameters of Perforated Plate

In order to facilitate designers to quickly calculate the flow coefficient of a perforated plate and to pre-evaluate its ventilation performance in the design stage, the multiple regression method is adopted to establish the functional relationship between the flow coefficient of a perforated plate and its geometric parameters; however, unlike gender, nationality, skin color, etc., the perforation shape of the perforated plate is an attribute variable rather than a quantifiable numerical variable. In order to enhance the predictive effect of the regression model, it should be defined as a dummy variable in the regression analysis and then included alongside other independent variables. A dummy variable, also known as a nominal variable, is an artificial variable defined to reflect material attributes, and its value is generally 0 or 1. For example, a dummy variable reflecting gender can be 1 (male) or 2 (female). The introduction of dummy variables can reflect the effects of different attribute types on dependent variables, which will make the regression model a more complex but more accurate description of the problem [42]. Here, the perforation shape is introduced into the regression model as a dummy variable. The definitions of dummy variables L_1 and L_2 are shown in Table 2.

Table 2. Dummy variable definition of perforation shapes.

Perforation Shape	L_1	L_2
Circle	0	0
Square	0	1
Triangle	1	0

Multiple linear regression is used to fit the flow coefficient and the perforated plate geometric parameters, and the fitting formula is as follows:

$$C_\mathrm{d} = 0.742\alpha - 0.123L_1 - 0.098L_2 + 0.003D + 0.630 \tag{7}$$

where C_d represents the flow coefficient of the perforated plate, α (%) represents the perforation rate of the perforated plate. When $L_1 = 0$ and $L_2 = 0$, the corresponding regression model is suitable for predicting the flow coefficient of a circular perforated plate, d (mm) denotes the perforation size.

Moreover, the adjusted R^2 is 0.847, indicating that the regression fitting effect is good. The regression formula passes the F test (F = 40.206, $p < 0.05$), proving that the formula is significant overall. Figure 11 shows a comparison between the C_d values determined by CFD simulations (actual C_d) and those predicted by the regression model (predicted C_d). The majority of the data points accumulated in a 45° line, and the model fit was satisfactory, with the MAE and NRMSE of the predicted and actual C_d values being 0.023 and 3.4%, respectively.

The regression coefficient of the perforation rate is 0.742 ($p = 0.000 < 0.01$), and the regression coefficient of the perforation size is 0.003 ($p = 0.020 < 0.05$), indicating that both the perforation rate and perforation size have a considerable positive influence on the flow coefficient. However, the regression coefficients of L_1 and L_2 are -0.123 and -0.098 ($p = 0.000 < 0.01$), respectively, suggesting that square and triangular holes have a negative influence on the flow coefficient compared with circular holes, which is consistent with the results in Section 3.2, namely, the circular hole can obtain a larger flow coefficient.

Furthermore, the independent variable and dependent variable are normalized to eliminate the influence caused by the difference in property and dimension between different variables. The calculated standard regression coefficients of α, L_1, L_2, and D are 0.592, -0.484, -0.386, and 0.187, respectively, revealing that the geometric parameters of

perforated plates that have the greatest influence on flow coefficient are perforation rate, perforation shape, and size, in descending order.
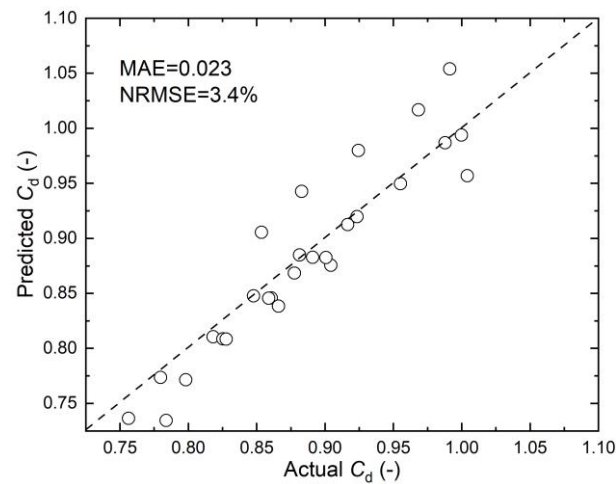

Figure 11. Comparison of the flow coefficient predicted by the regression model (predicted C_d) and calculated by CFD simulation (actual C_d).

4. Discussion

4.1. Application Analysis

As mentioned above, due to the lack of systematic research on the ventilation performance of perforated plates, architects are unable to pre-evaluate the ventilation performance during the design stage, which may result in poor natural ventilation during the building operation period. Therefore, this section explains how to use the regression model established in Section 3.4 to quickly select the type of perforated plate and calculate its flow coefficient in a practical engineering project. In the selection of a perforated plate, first of all, under the premise of consistent other conditions, using a circle hole can obtain a higher flow coefficient. Secondly, since the perforation size of the circular perforated plate has little influence on the flow coefficient, the designer can flexibly choose the perforation size in accordance with the requirements of the façade aesthetic. At the same time, the flow coefficient can be greatly enhanced by increasing the perforation rate while maintaining an aesthetic façade. To sum up, if a circular perforated plate with a perforation rate of 40% and size of 20 mm was finally selected for the building façade, its flow coefficient could be obtained as 0.987 by replacing it into Equation (7).

In addition, the perforated plate greatly increases the complexity of the geometric model and the computational cost in simulating the natural ventilation, but the flow coefficient can be used to simplify the building model. The detailed steps are as follows: in the first step, when modeling the geometry, the user only needs to establish the building walls and simple openings in the software, which means that the perforated plate can be removed. Then, as for boundary conditions, replace the boundary of pressure-inlet/outlet with inlet/outlet-vent for the perforated plate, and the pressure loss coefficient (ξ) needs to be defined at this boundary.

$$\xi = \frac{1}{C_d^2} \tag{8}$$

The flow coefficient of the perforated plate is 0.987, and the corresponding pressure loss coefficient can be calculated by Equation (8) as 1.03 so as to simplify the CFD simulation of natural ventilation of buildings with perforated plates.

4.2. Drawbacks and Future Works

Although this study investigated the influence of geometric parameters of the perforated plate on its flow coefficient by numerical simulation, there is still a lack of experiments

to effectively verify the simulation results, such as full-scale outdoor experiments or wind tunnel experiments. Therefore, the scientific impact of this study is limited by this drawback. Related studies have revealed that the wind direction also has a certain influence on the flow coefficient of the building openings [43]. However, due to the limitation of time, this study has not carried out the work in this aspect. In addition, the present study is limited to the ventilation performance of the perforated plate and the lack of comprehensive performance (thermal, ventilation, daylighting, and sun shading) evaluation of the perforated plate.

In the future, we will carry out a wind tunnel experiment in our climatic wind tunnel to measure the flow coefficient of the perforated plate, thus verifying our simulation results. On the basis of sufficient validation, the authors will investigate the quantitative relationship between the geometric parameters of the perforated plate on its comprehensive performance. As a result, a multi-objective optimization analysis should be required. Furthermore, perforated plates are gradually favored by architects, but the parameter module of perforated plates is not embedded in current energy simulation software at present (such as EnergyPlus) [41,44], which makes it difficult to consider its impact on building energy consumption directly. In the future, it can be implemented in the energy simulation software after the quantitative relationship between the geometric parameters on the comprehensive performance is established.

5. Conclusions

This study numerically examined the impact of the main geometric parameters (perforation rate, perforation size, and perforation shape) on the flow coefficient of the perforated plate, investigated the quantitative correlation between the flow coefficient and the geometric parameters, and explored the application value of the regression model in practical engineering. Several conclusions can be addressed:

(1) The flow coefficient of a perforated plate is not a constant, which increases with the increase in the perforation rate and is slightly greater than that of ordinary building openings.

(2) Under the same conditions, the corresponding flow coefficients of different holes rank as circle > square > triangle, and the circular hole can achieve higher flow coefficients and improve the effectiveness of natural ventilation.

(3) Given the assumption of constant perforation shape, the flow coefficient increases with the increase in the perforation size, and this effect is greater when the size is small. The flow coefficient is less affected by the size of round holes compared to triangular and square holes.

(4) The correlation between the flow coefficient and the geometric parameters of the perforated plate can be regressed by multiple linear functions, with the high precision of the adjusted R^2 being 0.847. Both the perforation rate and the perforation size have a considerable positive influence on the flow coefficient, while the square and triangle holes have a negative influence on the flow coefficient compared with the circular hole. Moreover, the geometric parameters of perforated plates that have the greatest influence on flow coefficient are perforation rate, perforation shape, and size, in descending order.

(5) The regression model can be used to select the type of perforated plate quickly and calculate its flow coefficient in a practical engineering project. By defining the pressure loss coefficient at the boundary, the model can also help simplify the geometric model in the simulation of building ventilation.

Author Contributions: Conceptualization, Y.P. and C.W.; methodology, Y.P.; software, H.M. and Z.L.; validation, Z.L. and Y.P.; writing—original draft preparation, Y.P. and H.M.; writing—review and editing, C.W. and H.M; visualization, Y.P. and Z.L.; supervision, C.W.; funding acquisition, C.W. All authors have read and agreed to the published version of the manuscript.

References

1. Cruz, H.; Viegas, J.C. On-site assessment of the discharge coefficient of open windows. *Energy Build.* **2016**, *126*, 463–476. [CrossRef]
2. Zhou, J.; Hu, Y.; Zhang, G. Unsteady characteristics of natural wind and its influence on indoor environment. *Sci. Technol. Rev.* **2012**, *30*, 62–68.
3. Yu, W.; Zhang, Y.; Du, C.; Li, B.; Liu, H.; Zhang, Y.; Wei, S. An innovative fan control strategy aimed at responding to human physiological characteristics for comfort sleeping. *Therm. Sci. Eng. Prog.* **2022**, *35*, 101470. [CrossRef]
4. Tan, K.; Qin, Y.; Wang, J. Evaluation of the properties and carbon sequestration potential of biochar-modified pervious concrete. *Constr. Build. Mater.* **2022**, *314*, 125648. [CrossRef]
5. Wang, J.; Meng, Q.; Yang, C.; Ren, P.; Santamouris, M. Spray optimization to enhance the cooling performance of transparent roofs in hot-humid areas. *Energy Build.* **2023**, *286*, 112929. [CrossRef]
6. Schulze, T.; Eicker, U. Controlled natural ventilation for energy efficient buildings. *Energy Build.* **2013**, *56*, 221–232. [CrossRef]
7. Bamdad, K.; Matour, S.; Izadyar, N.; Omrani, S. Impact of climate change on energy saving potentials of natural ventilation and ceiling fans in mixed-mode buildings. *Build. Environ.* **2022**, *209*, 108662. [CrossRef]
8. He, B.-J.; Zhao, D.; Dong, X.; Xiong, K.; Feng, C.; Qi, Q.; Darko, A.; Sharifi, A.; Pathak, M. Perception, physiological and psychological impacts, adaptive awareness and knowledge, and climate justice under urban heat: A study in extremely hot-humid Chongqing, China. *Sustain. Cities Soc.* **2022**, *79*, 103685. [CrossRef]
9. He, B.-J.; Zhao, D.; Dong, X.; Zhao, Z.; Li, L.; Duo, L.; Li, J. Will individuals visit hospitals when suffering heat-related illnesses? Yes, but . . . . *Build. Environ.* **2022**, *208*, 108587. [CrossRef]
10. Gil-Baez, M.; Barrios-Padura, A.; Molina-Huelva, M.; Chacartegui, R. Natural ventilation systems in 21st-century for near zero energy school buildings. *Energy* **2017**, *137*, 1186–1200. [CrossRef]
11. Ding, Y.; Li, B.; Shen, Y.; Su, Y. Numerical simulation of the effect of building layout and orientation on indoor natural ventilation. *Civ. Archit. Environ. Eng.* **2010**, *32*, 90–95.
12. Cardinale, N.; Micucci, M.; Ruggiero, F. Analysis of energy saving using natural ventilation in a traditional Italian building. *Energy Build.* **2003**, *35*, 153–159. [CrossRef]
13. Iqbal, A.; Afshari, A.; Wigo, H.; Heiselberg, P. Discharge coefficient of centre-pivot roof windows. *Build. Environ.* **2015**, *92*, 635–643. [CrossRef]
14. ASHRAE. *Handbook of Fundamentals*; American Society of Heating, Refrigerating and Air Conditioning Engineers (ASHRAE): Peachtree Corners, GA, USA, 2001.
15. Hunt, G.R.; Linden, P.P. The fluid mechanics of natural ventilation—Displacement ventilation by buoyancy-driven flows assisted by wind. *Build. Environ.* **1999**, *34*, 707–720. [CrossRef]
16. Li, Y.G.; Delsante, A.; Chen, Z.D.; Sandberg, M.; Andersen, A.; Bjerre, M.; Heiselberg, P. Some examples of solution multiplicity in natural ventilation. *Build. Environ.* **2001**, *36*, 851–858. [CrossRef]
17. Yi, Q.; Wang, X.; Zhang, G.; Li, H.; Janke, D.; Amon, T. Assessing effects of wind speed and wind direction on discharge coefficient of sidewall opening in a dairy building model—A numerical study. *Comput. Electron. Agric.* **2019**, *162*, 235–245. [CrossRef]
18. Liao, Q.; Guan, Y.; Wang, Q. Research of window's discharge coefficient in the natural ventilation room. In *Development of Industrial Manufacturing*; Trans Tech Publications Ltd.: Baech, Switzerland, 2014; pp. 420–426.
19. Wang, Y.; Yao, H.; Wen, F.; Chen, J. Analysis of the Building opening rate impact natural ventilation flow coefficient. *Ind. Build.* **2008**, *z1*, 67–69.
20. Chi, D.A.; Moreno, D.; Navarro, J. Impact of perforated solar screens on daylight availability and low energy use in offices. *Adv. Build. Energy Res.* **2021**, *15*, 117–141. [CrossRef]
21. Chi, D.A.; Moreno, D.; Navarro, J. Statistical methods applied to optimize perforated facade design for daylight availability. *J. Archit. Eng.* **2019**, *25*, 04018034. [CrossRef]
22. Blanco, J.M.; Arriaga, P.; Roji, E.; Cuadrado, J. Investigating the thermal behavior of double-skin perforated sheet facades: Part A: Model characterization and validation procedure. *Build. Environ.* **2014**, *82*, 50–62. [CrossRef]
23. Zapico, A.; Egiluz, Z.; Frometa, Y.G.; Cuadrado, J. Mechanical characterization of double-skin perforated-sheet facades. *J. Build. Eng.* **2022**, *56*, 104750. [CrossRef]
24. Miguel, A.F. Characterization of fluid flow through perforated plates. *J. Porous Media* **2019**, *22*, 1439–1448. [CrossRef]

25. Basaran, T.; Inan, T. Experimental investigation of the pressure loss through a double skin facade by using perforated plates. *Energy Build.* **2016**, *133*, 628–639. [CrossRef]

26. Tanner, P.; Gorman, J.; Sparrow, E. Flow-pressure drop characteristics of perforated plates. *Int. J. Numer. Methods Heat Fluid Flow* **2019**, *29*, 4310–4333. [CrossRef]

27. Li, Y. Study on Ventilation Additional Resistance Characteristics of Perforated Plates. Master's Thesis, Southwest Jiaotong University, Chengdu, China, 2016.

28. Montazeri, H.; Montazeri, F. CFD simulation of cross-ventilation in buildings using rooftop wind-catchers: Impact of outlet openings. *Renew. Energy* **2018**, *118*, 502–520. [CrossRef]

29. Bazdidi-Tehrani, F.; Masoumi-Verki, S.; Gholamalipour, P. Impact of opening shape on airflow and pollutant dispersion in a wind-driven cross-ventilated model building: Large eddy simulation. *Sustain. Cities Soc.* **2020**, *61*, 102196. [CrossRef]

30. Shen, X.; Zhang, G.; Bjerg, B. Comparison of different methods for estimating ventilation rates through wind driven ventilated buildings. *Energy Build.* **2012**, *54*, 297–306. [CrossRef]

31. Evola, G.; Popov, V. Computational analysis of wind driven natural ventilation in buildings. *Energy Build.* **2006**, *38*, 491–501. [CrossRef]

32. Ramponi, R.; Blocken, B. CFD simulation of cross-ventilation for a generic isolated building: Impact of computational parameters. *Build. Environ.* **2012**, *53*, 34–48. [CrossRef]

33. Huang, S.F.; Ma, T.Y.; Wang, D.; Lin, Z.H. Study on discharge coefficient of perforated orifices as a new kind of flowmeter. *Exp. Therm. Fluid Sci.* **2011**, *25*, 2237–2246. [CrossRef]

34. Jin, T.; Tian, H.; Gao, X.; Liu, Y.; Wang, J.; Chen, H.; Lan, Y. Simulation and performance analysis of the perforated plate flowmeter for liquid hydrogen. *Int. J. Hydrogen Energy* **2017**, *42*, 3890–3898. [CrossRef]

35. Zhou, X.-M.; Wang, Z.-K.; Zhang, Y.-F. A simple method for high-precision evaluation of valve flow coefficient by computational fluid dynamics simulation. *Adv. Mech. Eng.* **2017**, *9*, 1687814017713702. [CrossRef]

36. Chen, C.; Zhou, H. Analysis of applied discharge coefficients of different types of ventilation devices based on CFD. *J. HVAC* **2018**, *48*, 87–91.

37. Li, F. Adaptive Design of Perforated Metal Skin in Hot-Humid Area. Master's Thesis, South China University of Technology, Guangzhou, China, 2012.

38. Gong, G.; Li, H.; Nie, M.; Xie, G.; Li, Y. Discussion on the resistance property of natural ventilation induced by wind force. *J. Hunan Univ.* **2004**, *31*, 84–88.

39. Heiselberg, P.; Svidt, K.; Nielsen, P.V. Characteristics of airflow from open windows. *Build. Environ.* **2001**, *36*, 859–869. [CrossRef]

40. Andersen, K.T. Inlet and Outlet Coefficients—A Theoretical Analysis. In Proceedings of the 5th International Conference on Air Distribution in Rooms ROOMVENT'96, Tokyo, Japan, 17–19 July 1996; Volume 1.

41. Srisamranrungruang, T.; Hiyama, K. Balancing of natural ventilation, daylight, thermal effect for a building with double-skin perforated facade (DSPF). *Energy Build.* **2020**, *210*, 109765. [CrossRef]

42. Bingol, D.; Xiyili, H.; Elevli, S.; Kilic, E.; Cetintas, S. Comparison of multiple regression analysis using dummy variables and a NARX network model: An example of a heavy metal adsorption process. *Water Environ. J.* **2018**, *32*, 186–196. [CrossRef]

43. Yi, Q.; Zhang, G.; Li, H.; Wang, X.; Janke, D.; Amon, B.; Hempel, S.; Amon, T. Estimation of opening discharge coefficient of naturally ventilated dairy buildings by response surface methodology. *Comput. Electron. Agric.* **2020**, *169*, 105224. [CrossRef]

44. Chi, D.A.; Moreno, D.; Navarro, J. Design optimisation of perforated solar facades in order to balance daylighting with thermal performance. *Build. Environ.* **2017**, *125*, 383–400. [CrossRef]